Letter

# Equal contribution of even-frequency and odd-frequency pairing to transport across normal metal–superconductor junctions

Shun Tamura,[1] Viktoriia Kornich ⬤,[1] and Björn Trauzettel[1,2]

[1]*Institute for Theoretical Physics and Astrophysics, University of Würzburg, D-97074 Würzburg, Germany*
[2]*Würzburg-Dresden Cluster of Excellence ct.qmat, D-97074 Würzburg, Germany*

Odd-frequency pairing is an unconventional type of Cooper pairing in superconductors related to the frequency dependence of the corresponding anomalous Green's function. We show by a combination of analytical and numerical methods that odd-frequency pairing is ubiquitously present in the current of Andreev-scattered particles across a junction formed by a normal metal (N) and a superconductor (S), even if the superconducting pairing is of conventional *s*-wave, spin-singlet type. We carefully analyze the conductance of NS junctions with different pairing symmetries (*s* wave, *p* wave, *d* wave). In all cases, we identify a generic equal balance of even- and odd-frequency pairing to the contributions related to Andreev reflection. This analysis shows in retrospect that the presence of odd-frequency pairing in electric currents across NS junctions is rather the rule, not the exception. This insight stems from an alternative approach of analyzing the transport problem of hybrid structures. It is based on the Kubo-Greenwood formula with direct access to symmetries of the anomalous Green's functions characterizing the superconducting pairing. We expect that our predictions substantially enrich the interpretation of transport data across NS junctions in many material combinations.

Introduction. The symmetry of the superconducting pairing potential (SPP) has been the central topic since its discovery. One important (but less investigated) aspect thereof is its frequency dependence. The frequency dependence of the SPP is classified in two distinct ways: even- and odd-frequency pairing. Even-frequency pairing (EFP) applies to all known bulk superconductors to date, no matter whether their pairing is of conventional *s*-wave, spin-singlet type or unconventional. Odd-frequency pairing (OFP) is considered to be rather exotic. It refers to the property that the anomalous Green's function (related to a particular type of pairing amplitude) is odd under the exchange of time or frequency [1–5]. Bulk OFP has not yet been discovered experimentally. In fact, its stability is an interesting research topic by itself [6–10]. In hybrid structures, such as normal metal (N)–superconductor (S) junctions or Josephson junctions, translation symmetry is broken. It has been soon realized that this broken symmetry gives rise to the emergence of odd-frequency pairing in superconducting hybrids [11–17]. In Josephson junctions, supplemented with magnetic materials in the weak link, a long-range proximity effect has been considered as an indirect evidence of OFP [18]. More distinct features of OFP (as compared to EFP) have also been predicted, for instance, the paramagnetic Meissner effect, which should appear under certain conditions [19–23]. Indirect evidence of this particular type of attraction of magnetic flux by superconductivity has been reported in experiments based on low-energy muon spectroscopy [24–26] and on scanning tunneling spectroscopy (STS) [27,28].

However, it is fair to say that the present-day understanding is that it is difficult to observe evidence for OFP in any type of experiment involving superconductors or hybrid junctions

thereof. In this Letter, we argue that the opposite is true for standard transport measurements across NS junctions. In such junctions, it is impossible to observe genuine fingerprints of conventional EFP. In fact, we show below that the transport features related to superconductivity, i.e., Andreev reflection in the context of NS junctions, are always equally balanced by EFP and OFP contributions. This observation is deeply connected to the underlying symmetries of retarded and advanced Green's functions that enter into linear response expressions for the conductance. It has been overlooked so far, because common methods of calculating these transport properties do not give insight on the impact of EFP or OFP on the conductance. We benchmark our discovery by a number of examples, where the N side is either a one-dimensional (1D) system or a 1D ladder and the S side is either a 1D or a 2D superconductor with different pairing symmetries such as *s* wave, *p* wave, and *d* wave. We expect that our predictions substantially enrich the interpretation of transport data across NS junctions in many material combinations.

Conductance across NS junction. We evaluate the conductance G by linear response theory employing

$$G = -\int dE \frac{df(E)}{dE} \bar{\Gamma}_e(E), \quad \Gamma_e(x, x', E) = \gamma(\tilde{G}, \tilde{G}), \quad (1)$$

$$\gamma(g_1, g_2) = \alpha \text{Tr}[P_e g_1(x, x', E) \overleftrightarrow{\nabla} \overleftrightarrow{\nabla}' g_2(x', x, E)]. \quad (2)$$

The spatial average is depicted by using the symbol of the overbar in this Letter: $\bar{\beta} = \frac{1}{(L_2-L_1)^2} \int_{L_1}^{L_2} dx dx' \beta(x, x')$. Here, $\alpha = \frac{-e^2\hbar^3\pi}{4m^2}$, $f(E)$ is the Fermi-Dirac distribution function, $g(x) \overleftrightarrow{\nabla} h(x) = [\partial_x g(x)]h(x) - g(x)\partial_x h(x)$, $\overleftrightarrow{\nabla}'$ acts on x', $P_e = (\hat{\tau}_0 + \hat{\tau}_3)/2$ with Pauli matrices $\hat{\tau}_{j=0,1,2,3}$ in

particle-hole space, m is an electron mass, e is an elementary charge, and the trace is taken for particle-hole and spin space. $\tilde{G}$ is given by $\tilde{G}(x, x', E) = \frac{1}{2\pi i}[\check{G}^A(x, x', E) - \check{G}^R(x, x', E)]$ with the advanced (retarded) Green's function (GF) $\check{G}^{A(R)}$. The symbol of the overtilde is used in this way throughout this Letter. Equation (1) in combination with Eq. (2) is known as the Kubo-Greenwood formula [29–31]. We evaluate $\bar{\Gamma}_e(E)$ in the N region, i.e., x and x' are chosen in the N region.

Dividing the GFs into normal and anomalous GFs described by $\check{G}_N$ and $\check{F}$, respectively, Andreev reflection is described by the anomalous part. Then, the retarded GF can be expressed as $\check{G}^R(x, x', E) = \begin{pmatrix} G_N^{R,11}(x,x',E) & F^{R,12}(x,x',E) \\ F^{R,21}(x,x',E) & G_N^{R,22}(x,x',E) \end{pmatrix}$ with

$$\check{G}^R(x, x', E)$$

$$= -i \int d(t - t') e^{i(E+i\eta)(t-t')} \Theta(t - t')$$

$$\times \begin{pmatrix} \langle \{\Psi_\sigma(x,t), \Psi_{\sigma'}^\dagger(x',t')\} \rangle & \langle \{\Psi_\sigma(x,t), \Psi_{\sigma'}(x',t')\} \rangle \\ \langle \{\Psi_\sigma^\dagger(x,t), \Psi_{\sigma'}^\dagger(x',t')\} \rangle & \langle \{\Psi_\sigma^\dagger(x,t), \Psi_{\sigma'}(x',t')\} \rangle \end{pmatrix},$$

(3)

where $\Theta(t)$ is the Heaviside step function, and $\check{G}_N^R$ and $\check{F}^R$ are normal and anomalous GFs: $\check{G}_N^R = \begin{pmatrix} G_N^{R,11} & 0 \\ 0 & G_N^{R,22} \end{pmatrix}$ and $\check{F}^R = \begin{pmatrix} 0 & F^{R,12} \\ F^{R,21} & 0 \end{pmatrix}$. The advanced GF is defined similarly. Here, $\Psi_\sigma(x, t)$ is the Heisenberg representation of an annihilation operator with spin σ, spatial position x, and time t. η is a positive infinitesimal number. $\bar{\Gamma}_e(E)$ can be divided into normal transmission $\bar{\Gamma}_N(E)$ and Andreev reflection $\bar{\Gamma}_F(E)$ terms,

$$\bar{\Gamma}_e(E) = \bar{\Gamma}_N(E) + \bar{\Gamma}_F(E),$$

(4)

with $\Gamma_N(x, x', E) = \gamma(\tilde{G}_N, \tilde{G}_N)$ and $\Gamma_F(x, x', E) = \gamma(\tilde{F}, \tilde{F})$. There are no cross terms between normal and anomalous GFs.

Even- and odd-frequency pairing contributions. In NS junctions, OFP induced at the interface can penetrate into the N region and contribute to Andreev reflection. We decompose $\Gamma_F(x, x', E)$ into EFP and OFP components. The advanced (retarded) GF can be written as the sum of even and odd components $\check{F}^{A(R)} = \check{F}^{A(R),\text{even}} + \check{F}^{A(R),\text{odd}}$. Then, Γ_F is decomposed as $\Gamma_F = \Gamma_F^{ee} + \Gamma_F^{oo} + \Gamma_F^{eo}$ with

$$\Gamma_F^{ee(oo)}(x, x', E) = \gamma(\tilde{F}^{\text{even(odd)}}, \tilde{F}^{\text{even(odd)}}),$$

(5)

$$\Gamma_F^{eo}(x, x', E) = \gamma(\tilde{F}^{\text{even}}, \tilde{F}^{\text{odd}}) + \gamma(\tilde{F}^{\text{odd}}, \tilde{F}^{\text{even}}).$$

(6)

We analyze the odd-frequency contribution to $\bar{\Gamma}_F(E)$ for three distinct systems illustrated in Fig. 1. Remarkably, we demonstrate that $\bar{\Gamma}_F^{ee}(E) = \bar{\Gamma}_F^{oo}(E)$ [32]. $\bar{\Gamma}_F^{eo}(E)$ is zero due to particle-hole symmetry [proof is given in the Supplemental Material (SM) [33]]. Hence, we do not discuss it. Figure 1(a) shows the continuum 1D NS junction, where we analytically prove the equal contribution of EFP and OFP to $\bar{\Gamma}_F(E)$. Figure 1(b) shows the 1D N/2D S junction inspired by scanning tunneling spectroscopy. In this setup, we analyze s-, p_x-, and d-wave SPPs. We demonstrate that only s-wave junctions exhibit Andreev reflection since both EFP and OFP vanish at the interface between 1D N and 2D S for p_x- and d-wave junctions. Hence, they cannot penetrate into the 1D N. These cancellations do not occur for the setup shown in Fig. 1(c), where the normal metal has more spatial structure.
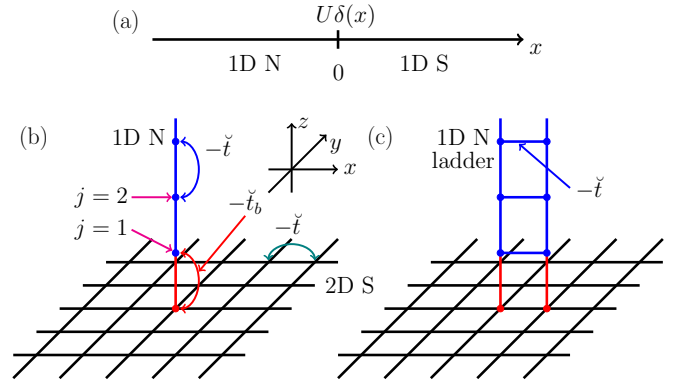

FIG. 1. Schematic illustration of three types of junctions. (a) Continuum 1D N/1D S junction, (b) 1D N/2D S lattice model, and (c) 1D N ladder/2D S lattice model.

1D N/1D S continuum model. We now present our analytical results for the 1D N/1D S continuum model. The Bogoliubov–de Gennes (BdG) Hamiltonian is $H(x, x') = \delta(x - x')\hat{\sigma}_0\hat{\tau}_3\varepsilon(x) + \Theta(x)\Theta(x')\Delta(x, x')$ with $\varepsilon(x) = -\frac{\hbar^2}{2m}\frac{d^2}{dx^2} - \mu + U\delta(x)$, μ the chemical potential, U the barrier potential at the interface, and $\hat{\sigma}_{j=0,1,2,3}$ Pauli matrices in spin space. As the SPP $\Delta(x, x')$, we study s-wave and p-wave cases: $\Delta(x, x') = \Delta\delta(x - x')i\hat{\sigma}_2 i\hat{\tau}_2$ for s wave, $\Delta(x, x') = \Delta\hat{\sigma}_1 \int dk \begin{pmatrix} 0 & e^{ik(x-x')} \\ -e^{-ik(x-x')} & 0 \end{pmatrix} \text{sgn}(k)$ for p wave [see also Fig. 1(a)]. We define the dimensionless parameter $Z = \frac{2mU}{k_F\hbar^2}$ with $k_F = \sqrt{\frac{2m\mu}{\hbar^2}}$. We derive the GFs along the lines of Refs. [34,35]. Explicit expressions are given in the SM [33]. Employing Eqs. (1) and (2), we reproduce the differential conductance of Blonder, Tinkham, and Klapwijk (BTK) theory [36,37], $\bar{\Gamma}_N(E) = \frac{e^2}{\pi\hbar}[1 - |b(E)|^2]$ and $\bar{\Gamma}_F(E) = \frac{e^2}{\pi\hbar}\frac{k_h}{k_e}|a(E)|^2$, where the electron (hole) wave number is given by $k_{e(h)} = \sqrt{\frac{2m}{\hbar^2}[\mu + (-)E]}$, and $a(E)$ and $b(E)$ are hole (Andreev) and electron reflection coefficients, respectively. We choose $L_1 = -\infty$ and $L_2 = 0$.

The EFP and OFP contributions are

$$\frac{4\pi\hbar}{e^2}\Gamma_F^{ee(oo)}(x, x', E)$$

$$= \frac{k_h}{k_e}|a(E)|^2 + \frac{k_e}{k_h}|a(-E)|^2$$

$$- (+)\frac{(k_e + k_h)^2}{2k_e k_h}\text{Re}\left[a(E)a^*(-E)e^{-i(k_e-k_h)(x+x')}\right]$$

$$+ (-)\frac{(k_e - k_h)^2}{2k_e k_h}\text{Re}\left[a(E)a(-E)e^{-i(k_e+k_h)(x+x')}\right].$$

(7)

After averaging over x and x', the last two terms in Eq. (7) vanish. Then, we obtain $\bar{\Gamma}_F^{ee}(E) = \bar{\Gamma}_F^{oo}(E)$ for $E \neq 0$ [38] (see the SM [33] for further details). For the s-wave junction with a fully transparent barrier [$Z = 0$ shown Fig. 2(a)], perfect Andreev reflection occurs, and $\frac{2\pi\hbar}{e^2}\bar{\Gamma}_e(E) \sim 4$ holds for $|E| < |\Delta|$ [39]. As the value of Z increases [$Z = 1$ and $Z = 3$ shown in Figs. 2(b) and 2(c), respectively], the shape of $\bar{\Gamma}_e(E)$ approaches the U-shaped density of states reflecting the s-wave SPP. Accordingly, the amplitude of Andreev reflection
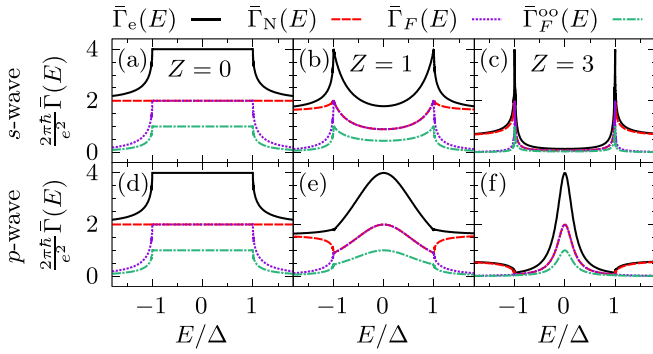
FIG. 2. $\bar{\Gamma}_e(E)$ and its components are plotted as a function of E for several values of $Z = 2mU/(k_F\hbar^2)$. (a)–(c) s-wave and (d)–(f) p-wave junctions. $Z = 0$ for (a) and (d), 1 for (b) and (e), and 3 for (c) and (f). $\Delta/\mu = 0.01$ for all plots.

is suppressed. For any values of Z, $\bar{\Gamma}_N(E) = \bar{\Gamma}_F(E)$ holds for $|E| < |\Delta|$ due to the normalization of the coefficients: $\frac{k_h}{k_e}|a(E)|^2 + |b(E)|^2 = 1$ for $|E| < |\Delta|$ [36]. The presence of Andreev reflection [$\bar{\Gamma}_F(E) \neq 0$] is thus inherently connected to the presence of OFP [40–45]. For p-wave junctions [Figs. 2(d)–2(f)], $\bar{\Gamma}_e(E = 0)$ takes a constant value due to the presence of a Majorana state [46–48]. Half of it stems from Andreev reflection $\bar{\Gamma}_F(E = 0)$. Experimental conductance exhibiting a zero energy peak larger than the value of the normal state signifies the existence of Andreev reflection, a distinct indicator of the presence of OFP. Hence, in Refs. [49–53], signatures of OFP have been observed in retrospect.

1D N/2D S lattice model. Let us now consider the model illustrated in Fig. 1(b). The Hamiltonian is given by

$$
\begin{aligned}
H = &-\check{t}\sum_{j>0,\sigma}(c_{j,\sigma}^\dagger c_{j+1,\sigma} + \text{H.c.}) - \mu_N\sum_{j>0,\sigma}c_{j,\sigma}^\dagger c_{j,\sigma}\\
&-\check{t}_b(c_{1,\sigma}^\dagger b_{\mathbf{j}_0,\sigma} + \text{H.c.}) + H_\Delta\\
&-\check{t}\sum_{\langle\mathbf{i},\mathbf{j}\rangle,\sigma}(b_{\mathbf{i},\sigma}^\dagger b_{\mathbf{j},\sigma} + \text{H.c.}) - \mu_S\sum_{\mathbf{j},\sigma}b_{\mathbf{j},\sigma}^\dagger b_{\mathbf{j},\sigma},
\end{aligned}
\tag{8}
$$

where $c_{j,\sigma}$ ($b_{\mathbf{j},\sigma}$) is an annihilation operator in 1D N (2D S) with the jth ($\mathbf{j}$th) site and spin σ. Here, $\check{t}$ is a hopping integral within 1D N and 2D S, $\check{t}_b$ is a hopping integral between 1D N and 2D S, $\mu_{N(S)}$ is a chemical potential in 1D N (2D S), and $\mathbf{j}_0 = (0,0)$. We utilize $\Delta/\check{t} = 0.1$, $\check{t}_b/\check{t} = 1$, $\mu_N/\check{t} = -0.5$, and $\mu_S/\check{t} = -1$. We impose periodic boundary conditions in the x direction with L_x sites and an infinite system in the y direction [54]. We consider s-, p_x-, and d-wave SPPs for $H_\Delta = \sum_{k,\sigma,\sigma'}b_{k,\sigma}^\dagger\hat{\Delta}_{\sigma,\sigma'}(k)b_{-k,\sigma'}^\dagger + \text{H.c.}$ with momentum k, where $\hat{\Delta}_{\sigma,\sigma'}(k)$ is given by $\Delta i\hat{\sigma}_2$, $\Delta\sin k_x\hat{\sigma}_3 i\hat{\sigma}_2$, and $\frac{\Delta}{2}(\cos k_x - \cos k_y)i\hat{\sigma}_2$, respectively. Without loss of generality, we assume that Δ is real and positive.

For the lattice model, we use a discretized version of Eq. (2): $\Gamma_e(j, j', E) = \pi\hbar\,\text{Tr}[\hat{P}_e\hat{J}_j\hat{\check{G}}_{j,j'}(E)\hat{J}_{j'}\hat{\check{G}}_{j',j}(E)]$ with $\hat{P}_e = \text{diag}(P_e, P_e)$, $\hat{J}_j = \begin{pmatrix}0 & J_{j,j+1}\\ J_{j+1,j} & 0\end{pmatrix}$, $J_{j,j+1} = J_{j+1,j}^* = \frac{e\check{t}}{i\hbar}\hat{\sigma}_0\hat{\tau}_0$, and $\hat{\check{G}}_{j,j'} = \begin{pmatrix}\check{G}_{j,j'} & \check{G}_{j,j'+1}\\ \check{G}_{j+1,j'} & \check{G}_{j+1,j'+1}\end{pmatrix}$ [55,56]. Here, the trace in $\Gamma_e(j, j', E)$ is taken for the spin, particle-hole, and neighboring two spatial lattice sites spanned from j to $j+1$. The spatial average is defined by $\bar{\Gamma}_e(E) = \frac{1}{L^2}\sum_{j,j'=1}^L\Gamma_e(j, j', E)$
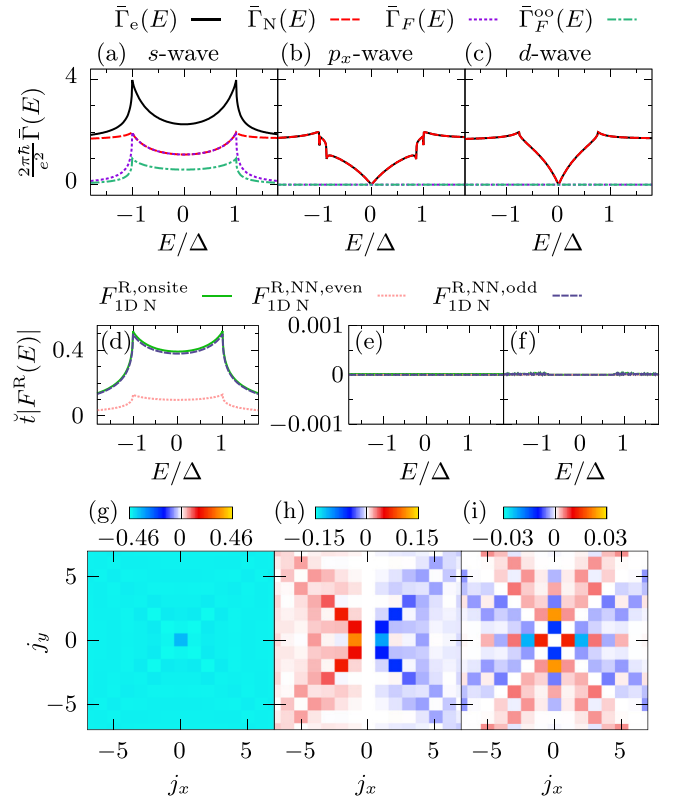

FIG. 3. (a)–(c) $\bar{\Gamma}_e(E)$ and its components are plotted as a function of E. $\bar{\Gamma}_F^{eo}(E) = 0$ numerically and is not plotted. (d)–(f) The absolute value of on-site and NN retarded GF in 1D N is plotted as a function of E. (a)–(f) Averaging length $L = 500$, $L_x = 10^7$, and $\eta/\check{t} = 10^{-7}$. (g)–(i) On-site component of the anomalous GF in Matsubara frequency representation in the 2D S close to the 1D N is plotted as functions of j_x and j_y with Matsubara frequency $\omega_n/\Delta = 0.1$ and $L_x = 2000$. (a), (d), and (g) s-wave, (b), (e), and (h) p_x-wave, and (c), (f), and (i) d-wave S junctions. (g) $\check{t}\,\text{Re}\,F_{2D,SS}^{\text{onsite,even}}$, (h) $\check{t}\,\text{Re}\,F_{2D,ST}^{\text{onsite,odd}}$, and (i) $\check{t}\,\text{Re}\,F_{2D,SS}^{\text{onsite,even}}$. The imaginary part for (g)–(i) is zero.

with j and j' chosen in the 1D N region. As shown in Figs. 3(a)–3(c), only the s-wave junction has a nonzero Andreev reflection [$\bar{\Gamma}_F(E) \neq 0$]. For p-wave and d-wave junctions, $\bar{\Gamma}_e(E)$ exhibits a V-shaped structure reflecting the density of states [57–59]. Numerical equivalence of $\bar{\Gamma}_F^{ee}$ and $\bar{\Gamma}_F^{oo}$ is shown in the SM [33]. The on-site ($j = 1$) and nearest-neighbor (NN) between $j = 1$ and $j = 2$ components [see Fig. 1(b)] of the retarded anomalous GF in the 1D N are plotted in Figs. 3(d)–3(f) [60]. In Figs. 3(d) and 3(f), s- and d-wave junctions, respectively, the spin-singlet (SS) EFP and OFP components are shown, and in Fig. 3(e), the p_x-wave junction, and the spin-triplet (ST) EFP and OFP components are shown [61]. In Fig. 3(d), we confirm that EFP and OFP penetrate into 1D N [62]. For p_x- and d-wave cases, both EFP and OFP do not penetrate into 1D N [Figs. 3(e) and 3(f)] [63].

Let us explain why EFP and OFP can (cannot) penetrate into 1D N for the s-wave (p_x- and d-wave) junction. As an example, the on-site components of the anomalous GF in 2D S close to 1D N are illustrated in Figs. 3(g)–3(i) (NN pairings are shown in the SM [33]). We define the on-site SS EFP

(ST OFP) component of the anomalous GF with Matsubara frequency (ω_n) in 2D S as follows,

$$
\begin{aligned}
&F_{\text{2D,SS(ST)}}^{\text{onsite,even(odd)}}(\mathbf{j}, i\omega_n) \\
&= \frac{1}{4}\sum_{\zeta=\pm 1} g(\zeta)\big[F_{\mathbf{j},\mathbf{j},\uparrow,\downarrow}^{12}(\zeta\, i\omega_n) - (+)F_{\mathbf{j},\mathbf{j},\downarrow,\uparrow}^{12}(\zeta\, i\omega_n)\big],
\end{aligned}
\quad (9)
$$

with $g(\pm 1) = 1$ for SS EFP and $g(\pm 1) = \pm 1$ for ST OFP [64]. When $F_{\text{2D,SS(ST)}}^{\text{onsite,even(odd)}}(\mathbf{j}_0, i\omega_n)$ is nonzero, the on-site pairing can penetrate into 1D N.

For the s-wave junction, the on-site anomalous GF (SS EFP) does not exhibit a sign change due to the isotropy of the s-wave SPP. Hence, this on-site pairing can penetrate into 1D N [Fig. 3(g)]. There are no cancellations for NN EFP and OFP. Thus, they can also penetrate into 1D N [Fig. 3(d)]. For the p_x-wave junction, the on-site anomalous GF (ST OFP) [Fig. 3(h)] exhibits a sign change at $j_x = 0$ since the p_x-wave SPP changes its sign in the $\pm x$ direction. Then, OFPs cancel each other at $j_x = 0$ and cannot penetrate into 1D N. For the d-wave S junction [Fig. 3(i)], the on-site anomalous GF (SS EFP) also exhibits a sign change at $j_x = \pm j_y$ reflecting d-wave symmetry. Then, the EFP contributions cancel each other and cannot penetrate into 1D N. For p_x-wave and d-wave junctions, NN EFP contributions also cancel each other and cannot penetrate into 1D N [33]. The same argument applies to NN OFP contributions.

1D N ladder/2D S model. From the results of the 1D N/2D S junctions, we expect that EFP and OFP can penetrate into the N lead if we replace the 1D N lead with a 1D N ladder [Fig. 1(c)]. Note that this setup mimics a double tip in STS experiments. The 1D N ladder is connected to $(j_x, j_y) = (0, 0)$ and $(1, 0)$. We plot $\bar{\Gamma}_e(E)$ and its components in Figs. 4(a)–4(c) accompanied with the on-site pairing of anomalous GFs in Figs. 4(d)–4(f) for p_x-, p_y-, and d-wave junctions. NN pairings are shown in the SM [33]. The SPP for the p_y-wave case is given by $\hat{\Delta}(k) = \Delta \sin k_y \hat{\sigma}_3 i\hat{\sigma}_2$. For p-wave junctions, depending on the orientation of SPPs (p_x or p_y wave), EFP and OFP can penetrate into the 1D N ladder. For the p_x-wave junction [Fig. 4(a)], we observe that EFP and OFP contribute to $\bar{\Gamma}_e(E)$ since on-site OFPs in the x direction do not cancel each other as shown in Fig. 4(d). However, for the p_y-wave junction [Fig. 4(b)], $\bar{\Gamma}_e(E)$ and its components are qualitatively the same as the ones in Fig. 3(b). Then, the OFP contributions cancel each other [Fig. 4(e)] (NN EFPs and NN OFPs also cancel and cannot penetrate into the 1D N ladder [33]). For the d-wave junction, shown in Fig. 4(c), EFP
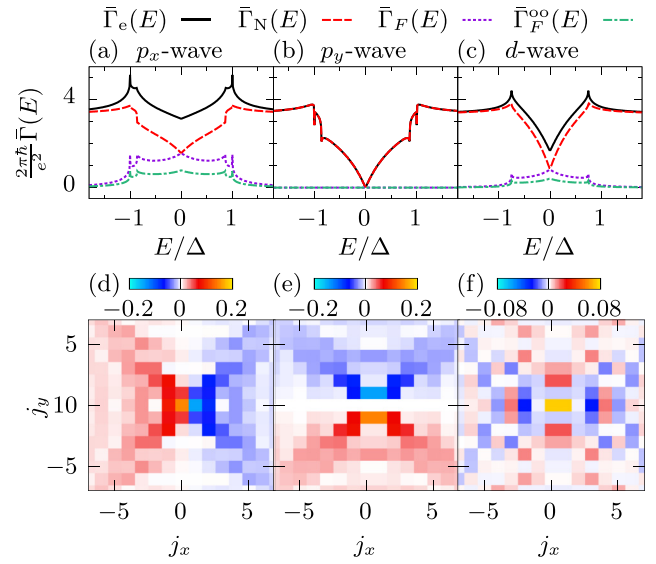

FIG. 4. (a)–(c) $\bar{\Gamma}_e(E)$ and its components are plotted as a function of E with $L = 500$, $L_x = 2\times 10^6$, and $\eta/\check{t} = 10^{-7}$. $\bar{\Gamma}_F^{\text{eo}}(E) = 0$ numerically and is not plotted. (d)–(f) On-site component of the anomalous GF close to the 1D N ladder is plotted as functions of j_x and j_y at $\omega_n/\Delta = 0.1$ with $L_x = 2000$. (a) and (d) p_x-wave, (b) and (e) p_y-wave, and (c) and (f) d-wave S junction. (d) and (e) $\check{t}\,\text{Re}\,F_{\text{2D,ST}}^{\text{onsite,odd}}$, (f) $\check{t}\,\text{Re}\,F_{\text{2D,SS}}^{\text{onsite,even}}$. The imaginary part for (d)–(f) is zero.

and OFP contribute to $\bar{\Gamma}_e(E)$, where the EFP contributions do not cancel each other [Fig. 4(f)].

Conclusions. We have analyzed the impact of even- and odd-frequency pairing on the conductance across generic NS junctions based on linear response theory. We have identified an equal balance of even- and odd-frequency pairing contributions to the conductance related to Andreev reflection. The larger the transparency across the junction, the more pronounced are these contributions typically. Hence, we prove that the presence of Andreev reflection in transport across NS junctions manifests the existence of odd-frequency pairing in a variety of hybrid structures.

[1] V. L. Berezinskii, New model of the anisotropic phase of superfluid He³, ZhETF Pis. Red. **20**, 628 (1974) [JETP Lett. **20**, 287 (1974)].

[2] Y. Tanaka, M. Sato, and N. Nagaosa, Symmetry and topology in superconductors—Odd-frequency pairing and edge states, J. Phys. Soc. Jpn. **81**, 011013 (2012).

[3] J. Linder and A. V. Balatsky, Odd-frequency superconductivity, Rev. Mod. Phys. **91**, 045005 (2019).

[4] J. Cayao, C. Triola, and A. M. Black-Schaffer, Odd-frequency superconducting pairing in one-dimensional systems, Eur. Phys. J.: Spec. Top. **229**, 545 (2020).

[5] C. Triola, J. Cayao, and A. M. Black-Schaffer, The role of odd-frequency pairing in multiband superconductors, Ann. Phys. **532**, 1900298 (2020).

[6] T. R. Kirkpatrick and D. Belitz, Disorder-induced triplet superconductivity, Phys. Rev. Lett. **66**, 1533 (1991).

[7] A. Balatsky and E. Abrahams, New class of singlet superconductors which break the time reversal and parity, Phys. Rev. B **45**, 13125 (1992).

[8] V. J. Emery and S. Kivelson, Mapping of the two-channel Kondo problem to a resonant-level model, Phys. Rev. B **46**, 10812 (1992).

[9] P. Coleman, A. Georges, and A. M. Tsvelik, Reflections on the one-dimensional realization of odd-frequency pairing, J. Phys.: Condens. Matter **9**, 345 (1997).

[10] S. Hoshino, J. Otsuki, and Y. Kuramoto, Diagonal composite order in a two-channel Kondo lattice, Phys. Rev. Lett. **107**, 247202 (2011).

[11] F. S. Bergeret, A. F. Volkov, and K. B. Efetov, Long-range proximity effects in superconductor-ferromagnet structures, Phys. Rev. Lett. **86**, 4096 (2001).

[12] Y. Tanaka and S. Kashiwaya, Anomalous charge transport in triplet superconductor junctions, Phys. Rev. B **70**, 012507 (2004).

[13] F. S. Bergeret, A. F. Volkov, and K. B. Efetov, Odd triplet superconductivity and related phenomena in superconductor-ferromagnet structures, Rev. Mod. Phys. **77**, 1321 (2005).

[14] Y. Tanaka, Y. Tanuma, and A. A. Golubov, Odd-frequency pairing in normal-metal/superconductor junctions, Phys. Rev. B **76**, 054522 (2007).

[15] Y. Tanaka and A. A. Golubov, Theory of the proximity effect in junctions with unconventional superconductors, Phys. Rev. Lett. **98**, 037003 (2007).

[16] Y. Asano and Y. Tanaka, Majorana fermions and odd-frequency Cooper pairs in a normal-metal nanowire proximity-coupled to a topological superconductor, Phys. Rev. B **87**, 104513 (2013).

[17] T. Löthman, C. Triola, J. Cayao, and A. M. Black-Schaffer, Disorder-robust p-wave pairing with odd-frequency dependence in normal metal–conventional superconductor junctions, Phys. Rev. B **104**, 094503 (2021).

[18] T. S. Khaire, M. A. Khasawneh, W. P. Pratt, and N. O. Birge, Observation of spin-triplet superconductivity in Co-based Josephson junctions, Phys. Rev. Lett. **104**, 137002 (2010).

[19] E. Abrahams, A. Balatsky, D. J. Scalapino, and J. R. Schrieffer, Properties of odd-gap superconductors, Phys. Rev. B **52**, 1271 (1995).

[20] S. Higashitani, Mechanism of paramagnetic Meissner effect in high-temperature superconductors, J. Phys. Soc. Jpn. **66**, 2556 (1997).

[21] S.-I. Suzuki and Y. Asano, Paramagnetic instability of small topological superconductors, Phys. Rev. B **89**, 184508 (2014).

[22] S.-P. Lee, R. M. Lutchyn, and J. Maciejko, Odd-frequency superconductivity in a nanowire coupled to Majorana zero modes, Phys. Rev. B **95**, 184506 (2017).

[23] F. Parhizgar and A. M. Black-Schaffer, Diamagnetic and paramagnetic Meissner effect from odd-frequency pairing in multiorbital superconductors, Phys. Rev. B **104**, 054507 (2021).

[24] A. Di Bernardo, Z. Salman, X. L. Wang, M. Amado, M. Egilmez, M. G. Flokstra, A. Suter, S. L. Lee, J. H. Zhao, T. Prokscha, E. Morenzoni, M. G. Blamire, J. Linder, and J. W. A. Robinson, Intrinsic paramagnetic Meissner effect due to s-wave odd-frequency superconductivity, Phys. Rev. X **5**, 041021 (2015).

[25] J. A. Krieger, A. Pertsova, S. R. Giblin, M. Döbeli, T. Prokscha, C. W. Schneider, A. Suter, T. Hesjedal, A. V. Balatsky, and Z. Salman, Proximity-induced odd-frequency superconductivity in a topological insulator, Phys. Rev. Lett. **125**, 026802 (2020).

[26] H. Alpern, M. Amundsen, R. Hartmann, N. Sukenik, A. Spuri, S. Yochelis, T. Prokscha, V. Gutkin, Y. Anahory, E. Scheer, J. Linder, Z. Salman, O. Millo, Y. Paltiel, and A. Di Bernardo, Unconventional Meissner screening induced by chiral molecules in a conventional superconductor, Phys. Rev. Mater. **5**, 114801 (2021).

[27] V. Perrin, F. L. N. Santos, G. C. Ménard, C. Brun, T. Cren, M. Civelli, and P. Simon, Unveiling odd-frequency pairing around a magnetic impurity in a superconductor, Phys. Rev. Lett. **125**, 117003 (2020).

[28] W. M. J. van Weerdenburg, A. Kamlapure, E. H. Fyhn, X. Huang, N. P. E. van Mullekom, M. Steinbrecher, P. Krogstrup, J. Linder, and A. A. Khajetoorians, Extreme enhancement of superconductivity in epitaxial aluminum near the monolayer limit, Sci. Adv. **9**, eadf5500 (2023).

[29] D. A. Greenwood, The Boltzmann equation in the theory of electrical conduction in metals, Proc. Phys. Soc. **71**, 585 (1958).

[30] H. U. Baranger and A. D. Stone, Electrical linear-response theory in an arbitrary magnetic field: A new Fermi-surface formation, Phys. Rev. B **40**, 8169 (1989).

[31] C. Caroli, R. Combescot, P. Nozieres, and D. Saint-James, Direct calculation of the tunneling current, J. Phys. C: Solid State Phys. **4**, 916 (1971).

[32] $\Gamma_e(x, x', E)$, $\Gamma_N(x, x', E)$, and $\Gamma_F(x, x', E)$ do not depend on x, and x' due to current conservation. However, $\Gamma_F^{ee}(x, x', E)$, and $\Gamma_F^{oo}(x, x', E)$ depend on x and x', and spatial averaging is needed.

[33] See Supplemental Material at http://link.aps.org/supplemental/10.1103/PhysRevB.109.L100505 for additional detailed derivation and numerical calculation, which includes Refs. [29,30,31,34–36,55,56,65].

[34] W. L. McMillan, Theory of superconductor—normal-metal interfaces, Phys. Rev. **175**, 559 (1968).

[35] C. Bruder, Andreev scattering in anisotropic superconductors, Phys. Rev. B **41**, 4017 (1990).

[36] G. E. Blonder, M. Tinkham, and T. M. Klapwijk, Transition from metallic to tunneling regimes in superconducting microconstrictions: Excess current, charge imbalance, and supercurrent conversion, Phys. Rev. B **25**, 4515 (1982).

[37] Y. Takane and H. Ebisawa, Conductance formula for mesoscopic systems with a superconducting segment, J. Phys. Soc. Jpn. **61**, 1685 (1992).

[38] At $E = 0$, the particle and hole momentum coincide ($k_e = k_h = k_F$), and the decomposition into EFP and OFP is not unique. On the other hand, for $E \neq 0$, the decomposition is unique.

[39] With an approximation $k_e = k_h = k_F$, $\frac{2\pi\hbar}{e^2}\bar{\Gamma}_e(E)$ is exactly 4 for $|E| < |\Delta|$, but without this approximation, it is not exactly 4, where $\frac{2\pi\hbar}{e^2}\bar{\Gamma}_e(E) \to 4$ for $|E| < |\Delta|$ when $\Delta/\mu \to 0$.

[40] S. Lee, V. Stanev, X. Zhang, D. Stasak, J. Flowers, J. S. Higgins, S. Dai, T. Blum, X. Pan, V. M. Yakovenko, J. Paglione, R. L. Greene, V. Galitski, and I. Takeuchi, Perfect Andreev reflection due to the Klein paradox in a topological superconducting state, Nature (London) **570**, 344 (2019).

[41] P. Parab, D. Singh, S. Haram, R. P. Singh, and S. Bose, Point contact Andreev reflection studies of a non-centrosymmetric superconductor Re$_6$Zr, Sci. Rep. **9**, 2498 (2019).

[42] R. J. Soulen, J. M. Byers, M. S. Osofsky, B. Nadgorny, T. Ambrose, S. F. Cheng, P. R. Broussard, C. T. Tanaka, J. Nowak, J. S. Moodera, A. Barry, and J. M. D. Coey, Measuring the spin polarization of a metal with a superconducting point contact, Science **282**, 85 (1998).

[43] P. Zareapour, A. Hayat, S. Y. F. Zhao, M. Kreshchuk, Z. Xu, T. S. Liu, G. D. Gu, S. Jia, R. J. Cava, H.-Y. Yang, Y. Ran, and K. S. Burch, Andreev reflection without Fermi surface alignment in high-T_c van der Waals heterostructures, New J. Phys. **19**, 043026 (2017).

[44] J. A. Voerman, J. C. de Boer, T. Hashimoto, Y. Huang, C. Li, and A. Brinkman, Dominant s-wave superconducting gap in PdTe$_2$ observed by tunneling spectroscopy on side junctions, Phys. Rev. B **99**, 014510 (2019).

[45] I. Hwang, K. Lee, H. Jin, S. Choi, E. Jung, B. H. Park, and S. Lee, A new simple method for point contact Andreev reflection (PCAR) using a self-aligned atomic filament in transition-metal oxides, Nanoscale **7**, 8531 (2015).

[46] A. Y. Kitaev, Unpaired Majorana fermions in quantum wires, Phys. Usp. **44**, 131 (2001).

[47] S. Tamura, S. Nakosai, A. M. Black-Schaffer, Y. Tanaka, and J. Cayao, Bulk odd-frequency pairing in the superconducting Su-Schrieffer-Heeger model, Phys. Rev. B **101**, 214507 (2020).

[48] D. Kuzmanovski, A. M. Black-Schaffer, and J. Cayao, Suppression of odd-frequency pairing by phase disorder in a nanowire coupled to Majorana zero modes, Phys. Rev. B **101**, 094506 (2020).

[49] V. Mourik, K. Zuo, S. M. Frolov, S. R. Plissard, E. P. A. M. Bakkers, and L. P. Kouwenhoven, Signatures of Majorana fermions in hybrid superconductor-semiconductor nanowire devices, Science **336**, 1003 (2012).

[50] J.-P. Xu, M.-X. Wang, Z. L. Liu, J.-F. Ge, X. Yang, C. Liu, Z. A. Xu, D. Guan, C. L. Gao, D. Qian, Y. Liu, Q.-H. Wang, F.-C. Zhang, Q.-K. Xue, and J.-F. Jia, Experimental detection of a Majorana mode in the core of a magnetic vortex inside a topological insulator-superconductor Bi$_2$Te$_3$/NbSe$_2$ heterostructure, Phys. Rev. Lett. **114**, 017001 (2015).

[51] H.-H. Sun, K.-W. Zhang, L.-H. Hu, C. Li, G.-Y. Wang, H.-Y. Ma, Z.-A. Xu, C.-L. Gao, D.-D. Guan, Y.-Y. Li, C. Liu, D. Qian, Y. Zhou, L. Fu, S.-C. Li, F.-C. Zhang, and J.-F. Jia, Majorana zero mode detected with spin selective Andreev reflection in the vortex of a topological superconductor, Phys. Rev. Lett. **116**, 257003 (2016).

[52] H.-H. Sun and J.-F. Jia, Detection of Majorana zero mode in the vortex, npj Quantum Mater. **2**, 34 (2017).

[53] S. Heedt, M. Quintero-Pérez, F. Borsoi, A. Fursina, N. van Loo, G. P. Mazur, M. P. Nowak, M. Ammerlaan, K. Li, S. Korneychuk, J. Shen, M. A. Y. van de Poll, G. Badawy, S. Gazibegovic, N. de Jong, P. Aseev, K. van Hoogdalem, E. P. A. M. Bakkers, and L. P. Kouwenhoven, Shadow-wall lithography of ballistic superconductor–semiconductor quantum devices, Nat. Commun. **12**, 4914 (2021).

[54] We utilize the recursive Green's function method [65] to calculate the Green's function. Then, the system can be infinite in one direction, but we must impose periodic or open boundary conditions in other directions.

[55] D. S. Fisher and P. A. Lee, Relation between conductivity and transmission matrix, Phys. Rev. B **23**, 6851 (1981).

[56] P. A. Lee and D. S. Fisher, Anderson localization in two dimensions, Phys. Rev. Lett. **47**, 882 (1981).

[57] S. H. Pan, J. P. O'Neal, R. L. Badzey, C. Chamon, H. Ding, J. R. Engelbrecht, Z. Wang, H. Eisaki, S. Uchida, A. K. Gupta, K.-W. Ng, E. W. Hudson, K. M. Lang, and J. C. Davis, Microscopic electronic inhomogeneity in the high-T_c superconductor Bi$_2$Sr$_2$CaCu$_2$O$_{8+x}$, Nature (London) **413**, 282 (2001).

[58] O. Fischer, M. Kugler, I. Maggio-Aprile, C. Berthod, and C. Renner, Scanning tunneling spectroscopy of high-temperature superconductors, Rev. Mod. Phys. **79**, 353 (2007).

[59] K. Fujita, A. R. Schmidt, E.-A. Kim, M. J. Lawler, D. Hai Lee, J. C. Davis, H. Eisaki, and S.-i. Uchida, Spectroscopic imaging scanning tunneling microscopy studies of electronic structure in the superconducting and pseudogap phases of cuprate high-T_c superconductors, J. Phys. Soc. Jpn. **81**, 011005 (2012).

[60] In Figs. 3(d)–3(f), $F_{1\text{D N}}^{\text{R,onsite}}$ and $F_{1\text{D N}}^{\text{R,NN,even(odd)}}$ are defined as follows. For s- and d-wave junctions, the on-site component is SS s-wave EFP,

$$F_{1\text{D N,SS}}^{\text{R,onsite}}(E) = \tfrac{1}{2}\big[F_{1,1,\uparrow,\downarrow}^{\text{R,12}}(E) - F_{1,1,\downarrow,\uparrow}^{\text{R,12}}(E)\big],$$

and the NN components are SS s-wave EFP and SS p-wave OFP,

$$F_{1\text{D N,SS}}^{\text{R,NN,even(odd)}}(E) = \tfrac{1}{4}\big[F_{1,2,\uparrow,\downarrow}^{\text{R,12}}(E) - F_{1,2,\downarrow,\uparrow}^{\text{R,12}}(E)\big]$$
$$+ (-)\tfrac{1}{4}\big[F_{1,2,\uparrow,\downarrow}^{\text{A,12}}(-E) - F_{1,2,\downarrow,\uparrow}^{\text{A,12}}(-E)\big].$$

For p-wave junctions, the on-site component is ST s-wave OFP,

$$F_{1\text{D N,ST}}^{\text{R,onsite}}(E) = \tfrac{1}{2}\big[F_{1,1,\uparrow,\downarrow}^{\text{R,12}}(E) + F_{1,1,\downarrow,\uparrow}^{\text{R,12}}(E)\big],$$

and the NN components are ST p-wave EFP and ST s-wave OFP,

$$F_{1\text{D N,ST}}^{\text{R,NN,even(odd)}}(E) = \tfrac{1}{4}\big[F_{1,2,\uparrow,\downarrow}^{\text{R,12}}(E) + F_{1,2,\downarrow,\uparrow}^{\text{R,12}}(E)\big]$$
$$+ (-)\tfrac{1}{4}\big[F_{1,2,\uparrow,\downarrow}^{\text{A,12}}(-E) + F_{1,2,\downarrow,\uparrow}^{\text{A,12}}(-E)\big].$$

[61] Due to spin rotational symmetry, s-wave and d-wave junctions can only have SS components, and p-wave S junctions can only have ST components. For on-site pairings, the SS OFP is forbidden by Fermi-Dirac statistics.

[62] The EFP and OFP components of retarded GFs are not even and odd functions of E, respectively. EFP and OFP satisfy $F^{\text{R,even}}(E) = F^{\text{A,even}}(-E)$ and $F^{\text{R,odd}}(E) = -F^{\text{A,odd}}(-E)$, respectively.

[63] The numerical error for d-wave junctions is larger than that for p_x-wave junctions since EFP and OFP contributions between the x and y direction cancel each other for d-wave junctions. We adopt periodic boundary conditions in the x direction and infinite length in the y direction. When the system size in the x direction is finite, there is no perfect cancellation in the x and y direction [Fig. 3(f)]. However, for p_x-wave junctions, EFP and OFP in the $+x$ and $-x$ direction cancel. Hence, in this case, there is almost no finite-size effect [Fig. 3(e)].

[64] We use the Matsubara frequency representation to reduce finite-size effects. To calculate the GF in real space, we cannot access large L_x due to the limitation of numerical resources. For finite L_x, the finite-size effects of the GF reduce when we adopt the Matsubara frequency representation for not too small Matsubara frequency.

[65] A. Umerski, Closed-form solutions to surface Green's functions, Phys. Rev. B **55**, 5266 (1997).